Tellus (2002), 54B, 143–162
Printed in UK. All rights reserved

TELLUS
ISSN 0280–6509

Small-scale patterns of sulfate aerosol climate forcing simulated with a high-resolution regional climate model

By ANNICA M. L. EKMAN, *Department of Meteorology, Stockholm University, SE-10691 Stockholm, Sweden*

(Manuscript received 22 January 2001; in final form 29 October 2001)

ABSTRACT

A high-resolution, regional climate model (RCA2) is employed to evaluate direct and indirect radiative forcing patterns due to man-made sulfate aerosols over Europe and to examine the sensitivity of the results to the choice of model resolution. A simulation encompassing the whole year of 1993 is performed. The model includes an explicit parameterization of the atmospheric sulfur cycle where predicted cloud and precipitation parameters are utilized at each time step. The overall pattern of the monthly mean direct climate effect simulated by the regional climate model is similar to that obtained using global climate models. Calculations over 0.4 and 4.0° spatial resolution indicate that, for the climatic conditions simulated by the RCA2, correlations between small-scale variations of relative humidity and aerosol loading do not contribute substantially to the magnitude of the monthly mean optical thickness.

For the monthly mean indirect climate effect, the finer grid spacing in the RCA2 results in a pronounced spatial variability, not visible in global climate model simulations. An interesting question is whether this variability affects the estimated magnitude of the indirect climate effect. Calculations of the effective droplet radius (r_e) for 0.4 and 4° spatial resolution indicate a minor importance over the RCA2 model domain (the difference in r_e is less than 7%). The model generally underestimates the sulfate concentration within the boundary layer, whereas the magnitude of the simulated CDNC and r_e agrees well with aircraft measurements. Despite an underestimate of the absolute magnitude, the regional pattern of the modeled r_e resembles that observed by satellite. A number of sensitivity simulations demonstrate that the magnitude of the indirect radiative forcing is highly uncertain. In order to reduce the uncertainty, different parameterizations of the indirect effect should be evaluated in more detail versus measurements of, e.g., aerosol concentration and properties, CDNC, and r_e at various locations.

1. Introduction

Aerosols can affect the climate directly by scattering short-wave radiation back to space (Charlson et al., 1991) and indirectly by altering the cloud and precipitation processes to make the clouds brighter and more long-lived (Twomey, 1974; Albrecht, 1989). The sign of the average climate forcing due to anthropogenic sulfate aerosols is negative and the absolute magnitude has been estimated from global climate model simulations to be as large as, or possibly even exceed, the expected warming due to human-induced greenhouse gases (IPCC, 1996). However, the uncertainty in the estimates of sulfate aerosol forcing is very large, particularly for the indirect climate effect, since complicated microphysical and chemical processes are involved in the formation of cloud droplets (IPCC, 1996; Lohmann and Feichter, 1997).

A number of global climate models have been employed to study the direct and indirect radiative forcing due to anthropogenic sulfate aerosols (e.g.

* Corresponding author.
e-mail: annica@misu.su.se

for the direct effect: Charlson et al., 1991; Penner et al., 1998; Koch et al., 1999; the indirect effect: Jones and Slingo, 1996; both effects: Chuang et al., 1997; Feichter et al., 1997; Kiehl et al., 2000). They all show an unevenly distributed forcing pattern with the highest values over, or in the vicinity of, industrialized regions. Langmann et al. (1998) compared the radiative forcing due to man-made sulfate aerosols from two week-long regional model simulations over Europe with the corresponding radiative forcing obtained from year-long simulations with a global model. Different predictions of the local cloud amount between the regional and global model modified the forcing significantly. However, Langmann et al. did not examine whether the difference in predicted cloud cover between the regional and global climate model simulations was caused by the choice of horizontal resolution or by the difference in integration time.

In the present study, a simulation encompassing the whole year of 1993 is conducted with a high-resolution regional climate model (RCA2). An important aspect is to evaluate whether the simulated magnitude and pattern of radiative forcing due to man-made sulfate differ substantially from previous results obtained by global climate models. Haywood et al. (1997) and Haywood and Boucher (2000) pointed out that sub-grid scale ($\leqslant 2.8^\circ$) variations in relative humidity, sulfate and clouds may contribute substantially to the direct and indirect climate forcing. In order to study this issue, aerosol optical depth and effective cloud droplet radius are calculated for two different spatial resolutions, 0.4 and 4°.

In the RCA2, simulated values of cloud liquid water content, relative humidity and fractional cloud cover are utilized in the calculations of the atmospheric sulfur cycle and sulfate aerosol forcing at each time step. The model is evaluated versus in-situ measurements of sulfate, cloud droplet number concentration and effective droplet radius, as well as satellite observations of effective droplet radius, in order to examine not only the confidence in the estimated radiative forcing but also the ability of the model to reproduce key variables in the parameterizations over both daily and monthly timescales. The uncertainty in the pattern and magnitude of the indirect effect is also examined by conducting a number of sensitivity simulations.

2. Model

The calculations are carried out with the Rossby Centre Regional Atmospheric Climate Model (RCA2). RCA2 is a modified version of RCA1 (Rummukainen et al., 2001), which in turn is based on the operational limited area forecast model HIRLAM (Källén, 1996; Eerola et al., 1997). The model is a hydrostatic, primitive equation grid-point model with Eulerian advection and a leapfrog semi-implicit time integration (Simmons and Burridge, 1981). Horizontal resolution in the applied version is 0.4° and there are 16 vertical levels. The model top is at 10 hPa. ECMWF (European Centre for Medium-Range Weather Forecasts) data are used at the lateral boundaries. Sea surface temperatures are prescribed.

The main differences between RCA1 and RCA2 are a new cloud parameterization scheme (Rasch and Kristjánsson, 1998 for the stratiform condensation; Kain and Fritsch, 1990 for the convective part), a new turbulence parameterization (Cuxart et al., 2000) and an updated radiation scheme (Wyser et al., 1999, Räisänen et al., 2000). In the previous version of the radiation scheme, radiative transfer depended only on the prognostic water vapor and cloud fields, whereas the role of CO_2, ozone and background aerosol were incorporated as constants. The modification by Räisänen et al. allows for varying CO_2 and the addition by Wyser et al. allows the radiative transfer to be dependent on cloud droplet number concentration (CDNC). The latter feature is especially important for the present study of the indirect effect. The direct scattering by aerosols is strongly parameterized in the model and this limits us in the study of the direct climate effect, a matter to be discussed further in Section 2.1.

The modeled cloud field is an important parameter when climate effects due to human-induced sulfate are considered. A preliminary evaluation of the modeled monthly mean cloud cover versus observed Climatic Research Unit (CRU, New et al., 1999) data demonstrates that the difference between observed and simulated average cloud cover is in general less than 10% (Fig. 1). However, over France, the cloud field is systematically underestimated by the model.

In the model of the atmospheric sulfur cycle (Berge, 1993; Ekman, 2000) processes such as transport, deposition and chemistry are calculated

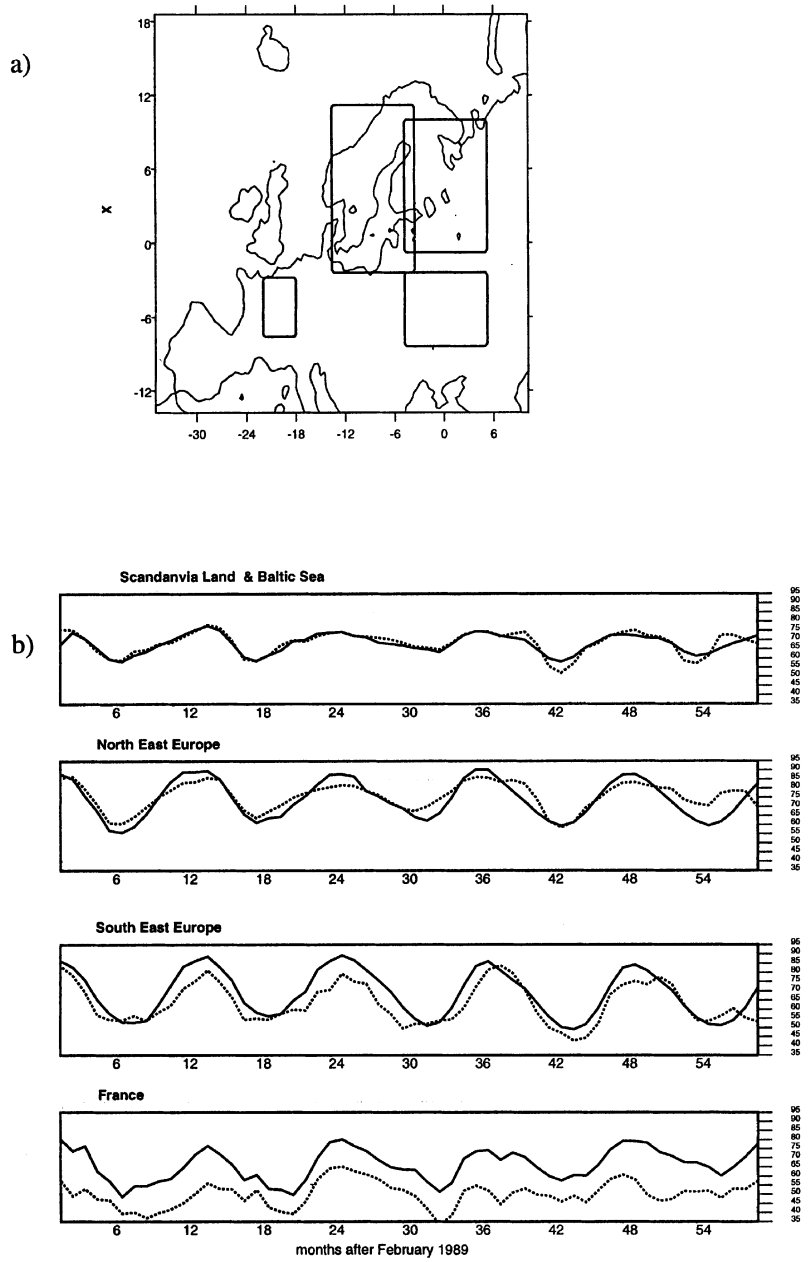

Fig. 1. Boxes showing designated regions (a) for which three-month running averages of monthly mean two-dimensional cloud cover (%) are calculated (b). Dotted line = RCA2 model. The first point shows a mean of Jan/Feb/March 1989 and the final point shows a mean of Oct/Nov/Dec 1993.

within the RCA2. Prognostic variables are sulfur dioxide in air (SO_2(a)), aerosol sulfate (SO_4(a)), sulfate in cloud water (SO_4(aq)) and hydrogen peroxide (H_2O_2). Emissions are obtained from the EMEP inventory (EMEP: Co-operative programme for monitoring and evaluation of the long-range transmission of air pollutants in Europe, Hjellbrekke and Hansen, 1998) and are, following Hass et al. (1996), assumed to reach the atmosphere as 95% SO_2(a) and 5% SO_4(a). Advection of the tracer compounds is performed with an Eulerian mass flux scheme (Bott, 1989a,b). Vertical diffusion is included for SO_2(a), SO_4(a) and H_2O_2, whereas it is omitted for SO_4(aq) since it is not included for cloud water. Convective vertical transport has not been included for any of the tracer compounds. A comparison with model simulations of ^{222}Rn transport by Mahowald et al. (1997) indicates that the absence of convective mixing may in summer result in an overestimate of SO_2(a) in the boundary layer by approximately 20% and an underestimate in the free troposphere by 40–80%. For sulfate, the effect of upward transport of aerosols inside the updraft core of a convective cloud is counteracted by a downward transport of unscavenged aerosol from the environment, resulting in a net transport of sulfate from the free troposphere to the boundary layer (Rasch et al., 2000). However, judging from Plate 3 in their paper, the supply of sulfate to the boundary layer from above due to convection is marginal compared to the production of sulfate by aqueous- and gaseous-phase oxidation of SO_2 in the same region.

Scavenging of dissolved SO_2(a) and SO_4(aq) is dependent on the formation of precipitation at each model level. The dry deposition flux of SO_2(a), SO_4(a) and H_2O_2 to the surface is assumed to be proportional to a dry deposition velocity (which differs from compound to compound; Table 1) and an estimate of the tracer compound concentration at 1 m (Berge, 1990). In the gas phase, SO_2(a) is oxidized by the hydroxyl radical (OH) to form SO_4(a). Dissolution of SO_2(a) in cloud water is calculated using Henry's law. In the aqueous phase, dissolved SO_2(a) is oxidized by ozone (O_3) and H_2O_2 to form SO_4(aq). When a cloud forms, all SO_4(a) is incorporated into the cloud water, and when a cloud evaporates all SO_4(aq) is released. H_2O_2 is calculated according to Barth et al. (2000) with an input of the monthly averages of the peroxy radical (HO_2), OH and photolysis rate of H_2O_2 obtained from simulations with the ECHAM global climate model (Roelofs et al., 1998). There is no diurnal variation of the oxidants. Seasonally constant O_3 concentrations are assumed, both horizontally and vertically (Berge, 1993). No natural emissions of sulfur are included in the model. Instead, a background concentration of 0.05 μg S kg^{-1} is prescribed everywhere as SO_4(a). At the boundaries, the sulfur concentrations are set to zero. The sensitivity of the model to the boundary conditions is examined in Section 4.3.

Table 1. *Dry deposition velocities in cm s^{-1}*

	Land	Water	Snow
SO_2(a)	0.6	0.8	0.1
SO_4(a)	0.2	0.2	0.2
H_2O_2	0.5	0.5	0.5

2.1. Direct climate effect

Since the RCA2 radiation scheme was designed for computational efficiency, it only considers two spectral ranges, one for the solar (short-wave, SW) and one for the thermal (long-wave, LW) part of the spectrum. The downward SW flux at the surface for a clear sky is calculated as

$$F^{\downarrow}_{\mathrm{SW,sfc}} = S\cos\theta\,\{1 - 0.024\cos(\theta)^{-0.5} - aa\cdot 0.11\cdot u_s(p_s)^{0.25} - as\times p_s/p_{00} \times (0.28/(1+6.43\cos\theta) - 0.07\alpha_*)\}, \quad (1)$$

where S is the top-of-the-atmosphere (TOA) solar flux, θ is the solar zenith angle, p_s is the surface pressure, $p_{00} = 1000$ hPa is a reference pressure, and α_* is the surface albedo. In the model, the net TOA SW radiative flux is given by the total amount of absorbed SW radiation (cf. Appendix). The pressure-scaled slant water vapor path is

$$u_s(p_s) = u(0, p_s)/\cos\theta$$
$$u(p_1, p_2) = \frac{1}{g}\times\int_{p_1}^{p_2} q\times\frac{p}{p_{00}}\,\mathrm{d}p. \quad (2)$$

where q is specific humidity (kg kg^{-1}). The second and third terms on the right-hand side of eq. (1) represent the effect of O_3 absorption for a typical total ozone column of 350 DU and the water vapor absorption, respectively. The last term

describes the effect of molecular Rayleigh scattering. The coefficients *aa* and *as* (in the reference version set to 1.2 and 1.25, respectively) represent crude parameterizations of the average effects of aerosol absorption and aerosol scattering. With *aa* and $as = 1$ (i.e. no aerosols), eq. (1) produces the upper envelope of observations made in clean air (Savijärvi, 1990). The values $aa = 1$ and $as = 1.9$ are representative for areas with background non-absorbing aerosols. Because of the crude representation of the aerosol scattering in the RCA2 model, the present study is focused more on the pattern rather than on the magnitude of direct climate forcing. The sign of the forcing should be correct since an increase of *as* in the model always results in a reduced net surface SW radiation flux.

In order to let the short-wave radiation calculations be dependent on the aerosol concentration in the model, the coefficient *as* is parameterized according to

$$as = 1 + ac \times (1 - e^{-\tau_{aerosol}}), \tag{3}$$

where $\tau_{aerosol}$ is the optical thickness due to all aerosols. The sulfur model only predicts anthropogenic sulfate and it is assumed that

$$\tau_{aerosol} = \tau_{bg} + \tau_{sulfate}, \tag{4}$$

where τ_{bg} and $\tau_{sulfate}$ are the optical thicknesses due to the background and man-made sulfate aerosols, respectively. The coefficient *ac* in eq. (3) is included in the model since test simulations have shown that if *as* is only made dependent on $e^{-\tau_{aerosol}}$, the resulting forcing is unrealistically low compared to previous simulations of the direct climate effect (Charlson et al., 1991; Chuang et al., 1997; Feichter et al., 1997; Langmann et al., 1998; Penner et al., 1998; Koch et al, 1999; Kiehl et al., 2000). The magnitude of *ac* is chosen to give a TOA clear-sky SW radiation of the RCA2 at various locations similar to that obtained using a 'stand-alone' version of the radiation parameterization applied in the NCAR Community Climate model CCM3 (Kiehl et al., 1998; the one-dimensional version is available at http://www.cgd.ucar.edu/cms/crm/). In particular, the formulation of *ac* is adjusted to give an accurate representation of the change in TOA clear-sky SW radiation for a doubling of the optical thickness at 50° latitude with a surface albedo of 0.2:

$$ac = 12.7(b_{SO_4^{2-}} + \tau_{bg}/\alpha)^2 + 5.7(b_{SO_4^{2-}} + \tau_{bg}/\alpha) + 2.1, \tag{5}$$

where $b_{SO_4^{2-}}$ is the column burden of sulfate (in g m^{-2}). It is difficult to choose a unique value for τ_{bg}, since its magnitude is dependent on many factors, e.g. time of the day, season, volcanic activity, location etc. From the World Climatic Program (1986) we have chosen $\tau_{bg} = 0.1$ to be representative of a background value for the atmospheric aerosol. The total optical depth due to sulfate aerosols is given by

$$\tau_{sulfate} = \int_0^{z_{top}} \sigma_{sp}\, dz, \tag{6}$$

where $\sigma_{sp} = \alpha m_{SO_4^{2-}}$ and $m_{SO_4^{2-}}$ is the mass concentration of SO_4(a) and SO_4(aq) in g m^{-3}. Various magnitudes of the scattering efficiency α have been suggested, but most values at low relative humidity (RH < 60%) and 550 nm wavelength fall in the range 3.6–7.5 m^2 g^{-1} (Charlson et al., 1999). The scattering efficiency is highly dependent on relative humidity. As an example, the direct radiative forcing by aerosols at 80% RH for the mid-Atlantic coast of the United States was roughly twice that of the dry aerosol (Kotchenruther et al., 1999). In the present study, the model denoted 2 in Kotchenruther et al. has been selected to describe the humidity factor for the scattering by aerosols:

$$\alpha = \alpha_{dry}\left[1 + a\left(\frac{RH}{100}\right)^b\right], \tag{7}$$

where α_{dry} is prescribed as 5 m^2 g^{-1} and the coefficients *a* and *b* are tuning parameters. For clean air, *a* and *b* are equal to 1.7 and 3.4, respectively. For polluted air, *a* is equal to 3.2 and *b* is equal to 3.8. The air mass is in the model considered 'clean' (corresponding to northerly or southerly flow in Kotchenruther et al.) if the sulfate aerosol concentration is less than 2 μg m^{-3} S-SO_4.

2.2. *Indirect climate effect*

The indirect climate effect is calculated by relating the sulfate mass to the scattering and transmission of short-wave radiation in clouds through

the effective cloud droplet radius:

$$r_{\mathrm{e,water}} = \left(\frac{3 \times LWC}{4\pi\rho_l k \times CDNC} \right)^{1/3}, \quad (8)$$

where LWC is the cloud liquid water concentration (calculated by the dynamical model at each time step and weighted by the cloud fraction), k is equal to 0.81 over sea and 0.69 over land (Martin et al., 1994). A minimum $r_{\mathrm{e,min}} = 4$ μm is prescribed in the model to avoid spurious effects for low cloud liquid water concentrations. CDNC is the cloud droplet number concentration that in the atmosphere is equal to the number of activated aerosol particles per unit volume. As in most other global and regional sulfur models, RCA2 does not predict aerosol number. Instead the CDNC (cm^{-3}) is parameterized to be dependent on the aerosol mass. In the present study, the relationship derived by Glantz and Noone (2000) is used:

$$CDNC = 87 \times \log_{10}\left[1 + \left(\frac{M_{\mathrm{amp}}}{0.32} \right)^2 \right], \quad (9)$$

where M_{amp} is total accumulation mode aerosol mass concentration (μg m^{-3}), in the present study equal to an aerosol background mass m_{bg} plus the mass of the man-made sulfate aerosols, which are assumed to be in the form $(NH_4)_2SO_4$. This parameterization resembles others used in previous climate modeling studies (e.g. Hegg, 1994; Jones et al., 1994; Martin et al., 1994; Boucher and Lohmann, 1995; Jones and Slingo, 1996), but that of Glantz and Noone has the advantage of using a physically based conversion algorithm (cf. Fig. 7 in the paper by Glantz and Noone for a plot of the relationship and a comparison versus previous studies). Values of m_{bg} over land and sea are based on measurements of aerosol background concentrations and are chosen to be 200 cm^{-3} (Pirjola et al., 1998; Patterson et al., 1980) and 50 cm^{-3} (Curry, 1986; Herman and Curry, 1984; Covert et al., 1996), respectively. The concentrations decrease with a scale height of 2 km over land and 1 km over ocean. The sensitivity of the model results to m_{bg} is examined in Section 4.2.

3. Results

Simulations have been undertaken for the whole year of 1993 with a 2-month spin-up time for the sulfur chemistry. In order to calculate the net radiative forcing caused by the man-made sulfate emissions, as defined by IPCC (1996), no feedback is allowed between the altered radiative flux and the model climate system. Hence, we only calculate the change of the top-of-the-atmosphere shortwave radiative flux due to the presence of anthropogenic sulfate aerosols while keeping all other climatological variables fixed. During the simulation, the radiation scheme is called twice at each time step; the first time with both background concentrations of aerosols and anthropogenic sulfate and the second time with only background aerosols (as a reference). The radiative fluxes obtained from the second call are used by the climate model. In Section 3.1, an evaluation of the sulfur model as well the parameterizations of the direct and indirect climate effects is first presented. After this, the calculated direct and indirect climate effects are evaluated in Sections 3.2 and 3.3, respectively.

3.1. *Evaluation versus in-situ measurements and satellite data*

3.1.1. Evaluation of simulated sulfate concentrations. Figure 2 shows scatter-plots of monthly averaged SO_4(a) concentrations measured at approximately 60 different EMEP-stations in Europe for the year 1993 (Hjellbrekke and Hanssen, 1998), versus the corresponding simulated values at the lowest model level and nearest grid-point. The model generally underestimates the SO_4(a) concentration giving the largest deviation from the one-to-one line in April and July. Ekman (2000) concluded that errors in the simulated cloud cover and precipitation are likely to be the largest contributors to the scatter seen in these figures. An additional oxidation process that converts SO_2(a) to SO_4(a) would decrease the bias. The decrease in sulfur emissions over Europe between 1993 and 1996 (approximately 17%, cf. Mylona 1999) also partly contribute to the underestimate of sulfate by the RCA2.

Unfortunately, no observations of sulfate were available to examine the model performance in the free troposphere and in the planetary boundary layer above the surface. Fig. 3 shows the simulated annual mean vertically integrated sulfate mass column for the model domain. The background value is approximately equal to 2 $\mathrm{mgSO_4\ m^{-2}}$ and the maximum value over

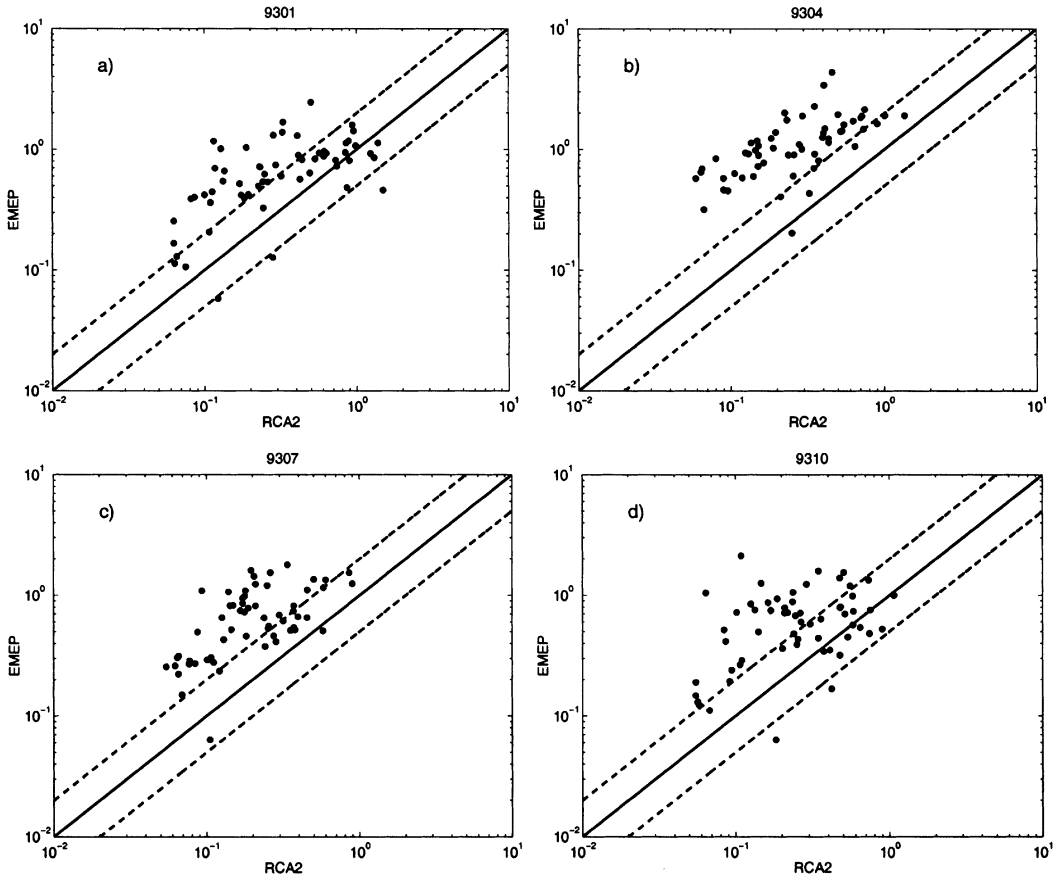

Fig. 2. Scatter plots between observed (surface) and simulated (lowest model level in the nearest grid-point) S-SO_4(a) concentrations during (a) January, (b) April, (c) July and (d) October. Concentrations are given in μg S kg^{-1}, the *x*-axis is the model and the *y*-axis is the observations. The 1:1 line (solid) and the 1:2 and 2:1 lines (dashed) are also shown.

Europe is estimated to be 7.0 $mgSO_4$ m^{-2}. These values are approximately a factor two lower than Charlson et al. (1991), Roeckner et al. (1999), Lohmann et al. (1999a,b) and Kiehl et al. (2000), mainly due to a large discrepancy in free tropospheric sulfate concentrations. One reason may be that the boundary values of sulfate are set to zero in the reference version of the RCA2 and that no convective vertical transport of sulfur compounds is included. Furthermore, the global climate models referred to above use emission data representative of the year 1985, or earlier, whereas the emission database utilized in the present study represents the year 1996. The anthropogenic sulfur emissions over Europe have been reduced substantially during the latest decades, from 1985 to 1996 by approximately 45% (Mylona, 1999).

3.3.2. Evaluation of modeled CDNC and $r_{e,water}$. A number of different parameterizations of the CDNC have been used in previous model studies (e.g. Hegg, 1994; Jones et al., 1994; Martin et al., 1994; Boucher and Lohmann, 1995; Jones and Slingo, 1996). They all assume, just as Glantz and Noone (2000) do for the parameterization used in the present study, that the aerosol or sulfate mass is uniquely related to the number of cloud droplets formed.

Table 2 shows the average of one surface series (Jennings et al., 1997) and two aircraft series of

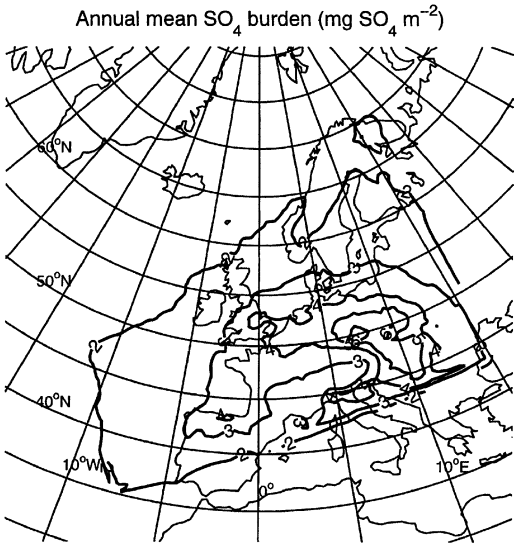

Fig. 3. Spatial distribution of the simulated annual mean anthropogenic sulfate aerosol burden (mg m^{-2}).

measured CDNC and $r_{e,water}$ (hereafter denoted r_e) (Choularton et al., 1998; Paul Field, personal communication) together with the corresponding modeled values. For the April case, the aircraft measurements took place between 9Z and 12Z and an average between the model results at 06Z and 12Z is used for the comparison. For the October case, the measurements were conducted over a shorter time period and we make use of the model output at 12Z. We have interpolated the CDNC to coincide with the average flight track height and thereafter chosen the concentration at the nearest grid-point. For the modeled r_e (r_e^m) , we chose the nearest model level with clouds. The surface measurements, representing a weekly average, are compared with the corresponding model average at the lowest model level nearest grid-point. All values of r_e^m and simulated CDNC correspond very well with the observations, cf. Table 2.

The three series of measurements of CDNC and r_e were all conducted over the British Isles and may not be representative for the rest of the model domain. In order to evaluate the model performance over regional scales, we compare r_e^m with satellite retrieval of r_e (r_e^s). Unfortunately, r_e^m cannot be evaluated in the same way as the observations. As seen by the results, this fact is problematic, and efforts should be made in the future to compare model results and satellite observations in a more consistent way.

The satellite data are obtained from the polar orbiting NOAA-11 satellite which passes over various parts of Europe at approximately 13.30 (local time) every day. Calculations of r_e^s are performed for clouds where the cloud tops are warmer than 273 K, i.e., generally low-level liquid water clouds not covered by ice clouds (Kawamoto et al., 2001). Cloud pixels with partial cloud cover and large cloud inhomogeneity are not included in the observations. Data with a 0.5° resolution are obtained by the satellite, but in order to emphasize the large-scale features, in the present study the data are averaged over $1° \times 1°$. From the model, estimates of r_e^m are obtained at every time step provided that the grid-box cloud fraction is larger than 1%. In each grid-column, the monthly mean r_e^m at the highest cloudy model

Table 2. *Observed and modeled (at 0.4° resolution) effective droplet radius,* r_e*, and cloud droplet number concentration, CDNC*[a,b] *(for further explanations, see text)*

Date	Average latitude	Average longitude	Average height (m)	CDNC (cm^{-3})		r_e (μm)	
				Obs	Model	Obs	Model
02/04/1993[c]	54.8°N	2.5°W	1423	172[a]	185	3.9[a]	4.6
28/10/1993[d]	51.0°N	6.1°W	1212	119[a]	125	6.2[a]	6.3
1/12/93–7/12/93[e]	53.2°N	9.5°W	Surface	96[b]	83	—	—

[a]Observations from Knollenberg forward scattering spectrometer probe.
[b]Observations from Twomey thermal diffusion chamber, CCN at 0.3% supersaturation.
[c]Field, personal communication.
[d]Choularton et al. (1998).
[e]Jennings et al. (1997).

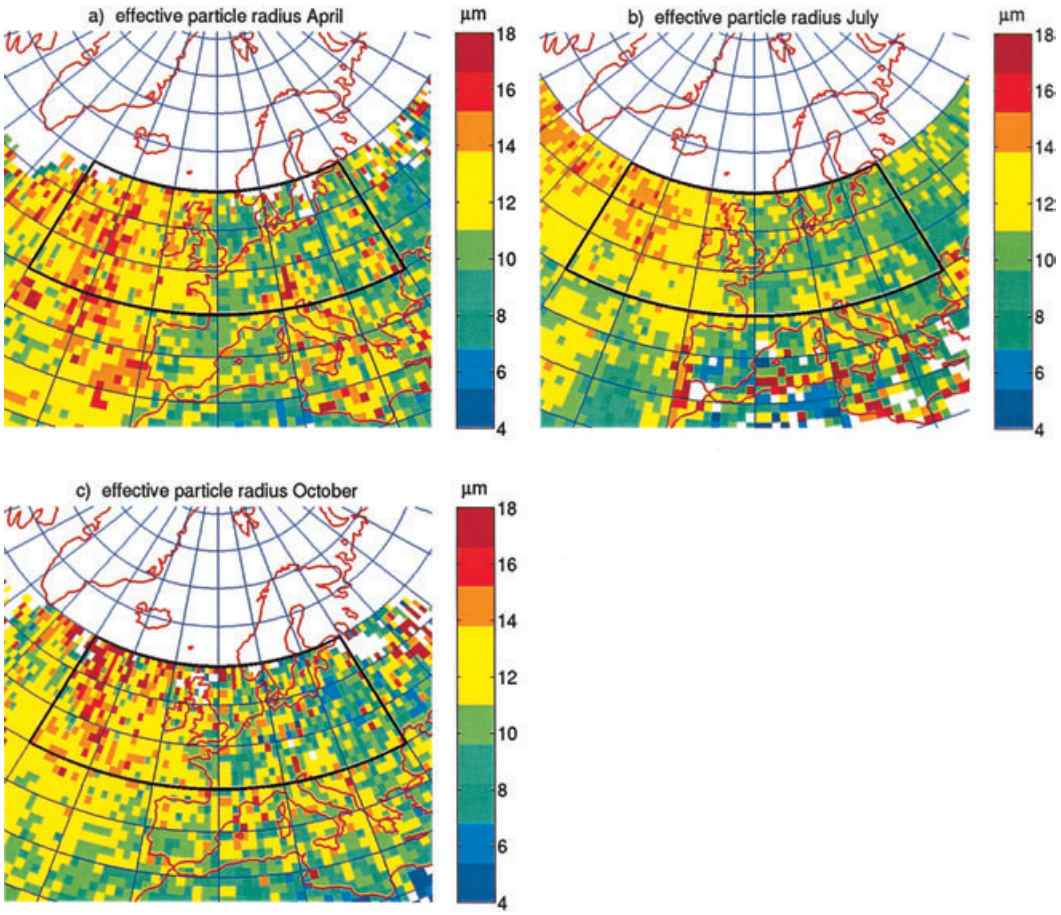

Fig. 4. Spatial distribution of satellite retrieved average effective droplet radius r_e (μm) for liquid water clouds ($\geqslant$273K) for (a) April, (b) July and (c) October. From Kawamoto et al. (2001). The area marked with black lines is suitable for comparison with the model simulation.

level, with a monthly average temperature warmer than 273 K, is used for the comparison.

Figures 4 and 5 show the geographical distribution of r_e^s and r_e^m for April, July and October. January is not shown since for this month the number of satellite retrieved data points over the model domain is low. The values of r_e^s are generally larger than the modeled. Thus, the plotted scales are different in order to make it easier to compare the patterns. We will return to the discrepancy in absolute magnitude of r_e later on in this subsection.

In the satellite data, a pronounced difference for all three months is seen between droplet radii over land and over ocean with higher values over the latter region. This pattern is also evident in the model simulations. Other interesting similarities between the modeled and satellite-retrieved large-scale patterns are that r_e generally is smaller over the North Sea than over the remote Atlantic, at least during April and October, that the largest r_e are found over the remote North Atlantic area and that the smallest r_e are found close to the eastern boundary of the marked area in the figures.

On smaller scales, there are some obvious discrepancies between model and observations. For example, in the model polluted air is advected from France and Spain out over the Atlantic Ocean in April and October resulting in small values of r_e^m over the Bay of Biscay and the eastern

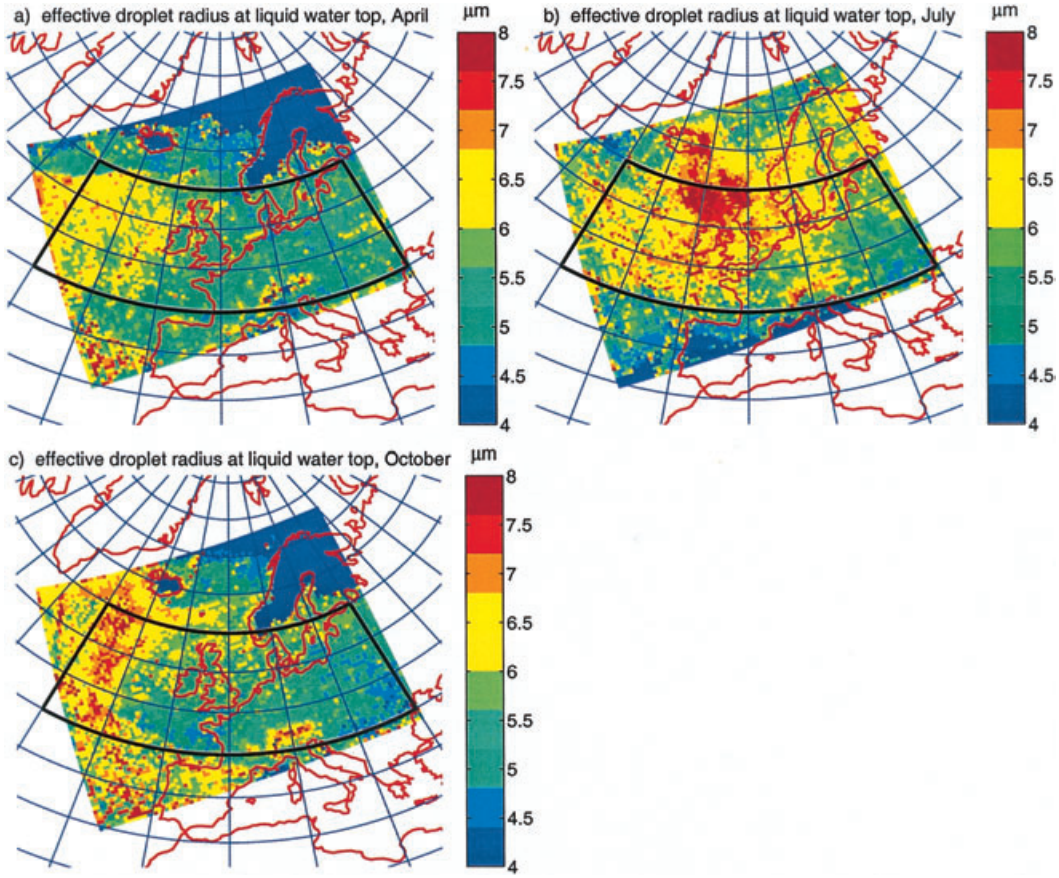

Fig. 5. Spatial distribution of simulated average effective droplet radius r_e (μm) for the highest model level with liquid water clouds for (a) April, (b) July and (c) October. The area marked with black lines is suitable for comparison with satellite observation.

Atlantic. This pattern is not evident in the satellite data. A closer look at the prevailing wind direction west of France and Spain shows that there are easterly or northeasterly winds approximately 15% and 50% of the days in April and October, respectively. Satellite data over the same region were only obtained for less than 2 of these days while the total number of days with data varied between approximately 4 and 12. Hence, a distribution with low values of r_e^s over the Bay of Biscay and eastern Atlantic may have been obscured by the dominance of observed days with westerly winds. In July, a maximum r_e^m, due to high cloud liquid water concentrations can be seen north of Scotland and Ireland. This maximum is not evident in the satellite data. There are no obvious reasons for the disagreement, but July 1993 was a period when a large number of low-pressure systems moved in from the Atlantic Ocean towards Europe. Errors in the modeled intensity and direction of these storm tracks may result in an erroneous distribution of liquid cloud water.

As noted earlier and seen in Figs. 4 and 5, the values of r_e^s are generally larger than the modeled. There are mainly two reasons why the magnitude of r_e differs between the two data sets. First of all, the model data show droplet radii from a certain model level whereas the satellite data show droplet radii representing the absolute top of a cloud. Due to the limited amount of vertical levels in the model, the altitude from which r_e^m are collected can be systematically lower compared to the

altitude where r_e^s are observed. Since r_e generally increases with height (e.g. Rosenfeld, 2000), the lower altitude of r_e^m compared to r_e^s should result in an underestimate bias by the model. Furthermore, cloud pixels with partial cloud cover and large cloud inhomogeneity are not included in the satellite observations, whereas they are considered in the model calculations. Low cloud fractions are generally associated with small droplet radii. Hence, the fact that the model in the calculations of r_e^m considers all types of clouds is also likely to result in an underestimate bias. In addition to the model domain averages of r_e^s and r_e^m for the reference case, Table 3 shows July estimates of r_e^m where model data are collected at the highest model level warmer than 263 K (instead of 273 K) and from grid-boxes with cloud fractions larger than 95% (instead of 1%). If these new conditions are employed, a large part of the discrepancy between the absolute value of r_e^s and r_e^m can be explained (cf. Table 3).

3.2. Direct climate effect

The direct climate forcing is dependent on the solar insolation and the difference between the sulfate column burden in the polluted atmosphere and that of the reference atmosphere. Due to the distribution of clouds and a larger sulfate burden compared to the other months, the maximum average forcing over the model domain occurs in May (Fig. 6). The calculated monthly and annual means in Fig. 6 and maxima in Table 4 are substantially lower (by a factor of 2–4) than those obtained in previous model studies (e.g. Charlson et al., 1991; Chuang et al., 1997; Feichter et al., 1997; Langmann et al., 1998; Penner et al., 1998; Koch et al, 1999; Kiehl et al., 2000). This discrepancy is caused by the large difference in free tropospheric concentrations of sulfate between the RCA2 and the other models (cf. Section 3.1.1). As mentioned before, we therefore focus our study on

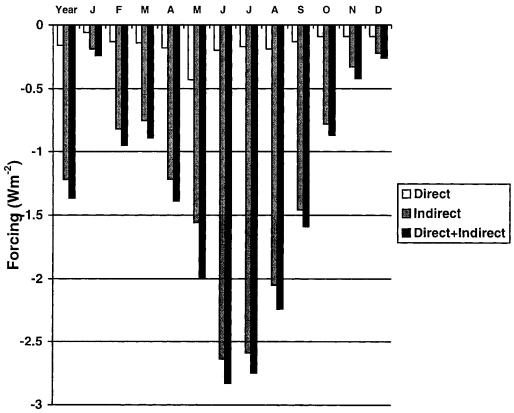

Fig. 6. Annual and monthly average direct, indirect and direct + indirect forcing (W m^{-2}) due to anthropogenic sulfate aerosols averaged over the RCA2 model domain.

Table 4. *Simulated maximum difference in net top-of-the-atmosphere short-wave radiation budget over the RCA2 model domain*

	Maximum direct forcing (W m^{-2})	Maximum indirect forcing (W m^{-2})
January	−0.8	−3.3
April	−2.0	−5.3
July	−1.6	−14.4
October	−1.1	−4.5
Annual mean	−1.3	−4.4

Table 3. *July average effective droplet radius (μm) derived from satellite (r_e^s) and from model (r_e^m)*

	$r_e^{s\,a}$	r_e^m *Clcov* > 1% *T* > 273 K (reference)	r_e^m *Clcov* > 1% *T* > 263 K	r_e^m *Clcov* ⩾ 95% *T* > 273 K	r_e^m *Clcov* ⩾ 95% *T* > 263 K
RCA2 domain	10.6	6.0	6.8	6.8	8.8
Ocean	11.2	6.0	6.6	6.9	9.1
Land	10.1	5.9	7.0	6.5	8.4

r_e^m is shown for four different conditions. *T* is monthly average temperature. *Clcov* is total cloud cover in each grid-box at each time-step of the model.
[a] From Kawamoto et al. (2001).

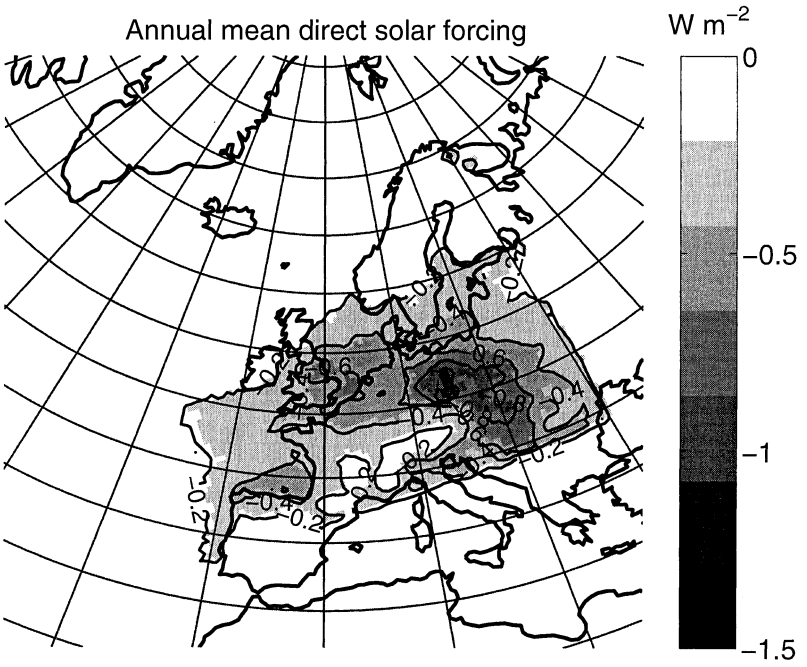

Fig. 7. Spatial distribution of the simulated annual mean direct climate forcing (W m^{-2}) due to anthropogenic sulfate aerosols.

the overall spatial pattern of the direct forcing rather than on the absolute value. Figure 7 shows the simulated annual mean geographical distribution of the direct aerosol radiative forcing due to human-induced sulfate. The maximum forcing is found close to the emission regions but it is extended towards the east because of the prevailing westerly winds. In the vicinity of the continental coastline, the radiative forcing is generally larger over ocean than over land, even though the land area is closer to the main emission areas. This phenomenon, which is especially evident north of Spain, is due to the dependence of the scattering efficiency on relative humidity [eq. (7)] and due to the difference in surface albedo over land and water. The gross pattern in many ways resembles that obtained in the global climate model study by Kiehl et al. (2000), which like the present study considers year-long averages of radiative forcing. In addition, the regional model is able to resolve some smaller-scale phenomena. For example, the annual mean direct forcing over the snow-covered Alps is very low because of the high surface albedo. This reduced forcing over mountain areas was also found in the regional climate model study by Langmann et al. (1998).

Correlations between small-scale spatial variations of relative humidity (RH) and sulfate, not resolved by global models, have been suggested as an uncertainty in the predictions of direct climate forcing (Haywood et al., 1997; Haywood and Boucher, 2000). The possible advantage of using highly resolved relative humidity and sulfate fields in the estimates of the direct climate effect is examined by calculating $\tau_{sulfate}$ [cf. eq. (6)] for two different spatial resolutions, 0.4° (as a reference) and 4°, respectively. The variables required to calculate $\tau_{sulfate}$ (RH and sulfate, where RH is calculated using temperature and specific humidity) at 4° resolution are obtained by averaging the results from the 0.4° resolution simulation over 10×10 grid-points. If monthly and yearly averages are considered in the comparison, $\tau_{sulfate}$ at 4° resolution may deviate from $\tau_{sulfate}$ at the finer grid spacing by 10–20% in individual grid-points (cf. the standard deviation in Table 5), $\tau_{sulfate}$ at the higher resolution generally being larger than $\tau_{sulfate}$ at the lower resolution. However, averaged

Table 5. *Monthly annual mean/standard deviation of optical thickness ($\tau_{sulfate}$) and effective droplet radius (r_e) over the RCA2 model domain, showing results at 0.4° and 4.0° resolution*

	$\tau_{sulfate} \times 10^3$ at 0.4° ave $\pm$ std	$\tau_{sulfate} \times 10^3$ at 4.0° ave $\pm$ std	r_e at 0.4° (μm) ave $\pm$ std	r_e at 4.0° (μm) ave $\pm$ std
January	13.5 ± 7.3	13.3 ± 6.4	9.1 ± 1.7	8.5 ± 1.7
February	14.6 ± 8.9	14.4 ± 7.7	8.9 ± 1.4	8.7 ± 1.2
March	14.3 ± 7.8	14.1 ± 6.9	8.3 ± 1.5	8.1 ± 1.4
April	14.7 ± 8.0	14.7 ± 7.5	8.6 ± 1.6	8.4 ± 1.6
May	20.3 ± 12.4	20.2 ± 11.7	8.3 ± 1.1	8.4 ± 0.8
June	14.4 ± 8.0	14.4 ± 7.5	9.3 ± 1.4	9.3 ± 1.2
July	13.9 ± 7.5	13.8 ± 7.0	9.5 ± 1.5	9.5 ± 1.3
August	14.6 ± 8.5	14.6 ± 8.1	9.7 ± 1.5	9.7 ± 1.2
September	13.9 ± 6.3	13.9 ± 5.9	9.4 ± 1.7	9.4 ± 1.6
October	13.0 ± 5.5	12.9 ± 4.8	9.3 ± 1.6	9.2 ± 1.4
November	15.1 ± 9.1	14.9 ± 7.8	8.8 ± 1.6	8.6 ± 1.6
December	13.0 ± 7.0	12.9 ± 6.2	9.6 ± 2.2	9.2 ± 2.2
Annual	14.9 ± 7.0	14.8 ± 6.6	8.9 ± 1.4	8.8 ± 1.4

over the model domain the difference is less than 5% (cf. Table 5). A possible cause of this small discrepancy in $\tau_{sulfate}$ is that the difference in RH standard deviation between the two resolutions is less than 1%. The results indicate that for the climatic conditions simulated by the RCA2, global climate models may only slightly underestimate the monthly mean direct climate effect due to missing correlations between small-scale variations of sulfate and RH.

3.3. *Indirect climate effect*

The maximum of the model domain average indirect radiative forcing due to man-made sulfate occurs in June and July (Fig. 6). Figure 8 shows the geographical distributions of the simulated monthly mean radiative forcing in January, April, July and October. Due to the low background concentration of sulfate, the maximum forcing during all months occurs over the ocean [cf. eq. (9)]. Furthermore, the type of clouds is important for the sensitivity. The spatial small-scale variations in forcing reflect largely the frequency of low-level clouds. For example, the large difference in TOA net short-wave radiation over the Norwegian Sea in July is a result of a prevailing stratiform cloud cover in the model. Also, low-level clouds occur more often well outside the coast of France and Spain compared to over the North Sea or the Baltic Sea.

One pronounced difference between the present study and the global climate model study by Kiehl et al. (2000), which also considers annual averages of radiative forcing, is that the spatial variability of the indirect climate effect is much larger in the RCA2. The magnitude of the average indirect forcing over Europe is however comparable. As the spatial variability persists over a long time period (more than a month), it should be the result of the higher horizontal resolution in the regional model rather than random variations. Langmann et al. (1998) reported similar spatial variability in their regional climate model calculations. However, in the simulations by Langmann et al. a part of the variability in the radiative forcing pattern may have been caused by the short time period considered (approximately a week).

In order to obtain an indication of whether correlations of small-scale spatial variations of liquid cloud water and sulfate (or CDNC) give a substantial contribution to the indirect climate forcing, the effective droplet radius, r_e [cf. eq. (8)], at the highest model level with liquid water clouds is calculated with variables obtained at both 0.4 and 4° horizontal resolutions. As in the comparison of $\tau_{sulfate}$ (cf. Section 3.2), the variables necessary to calculate r_e for the 4.0° resolution are obtained by averaging the results from the 0.4° resolution simulation over 10×10 grid-points. However, the comparison with different horizontal resolutions in the calculations of r_e is not as straightforward as the corresponding one performed for $\tau_{sulfate}$. When the averaging over 4° is

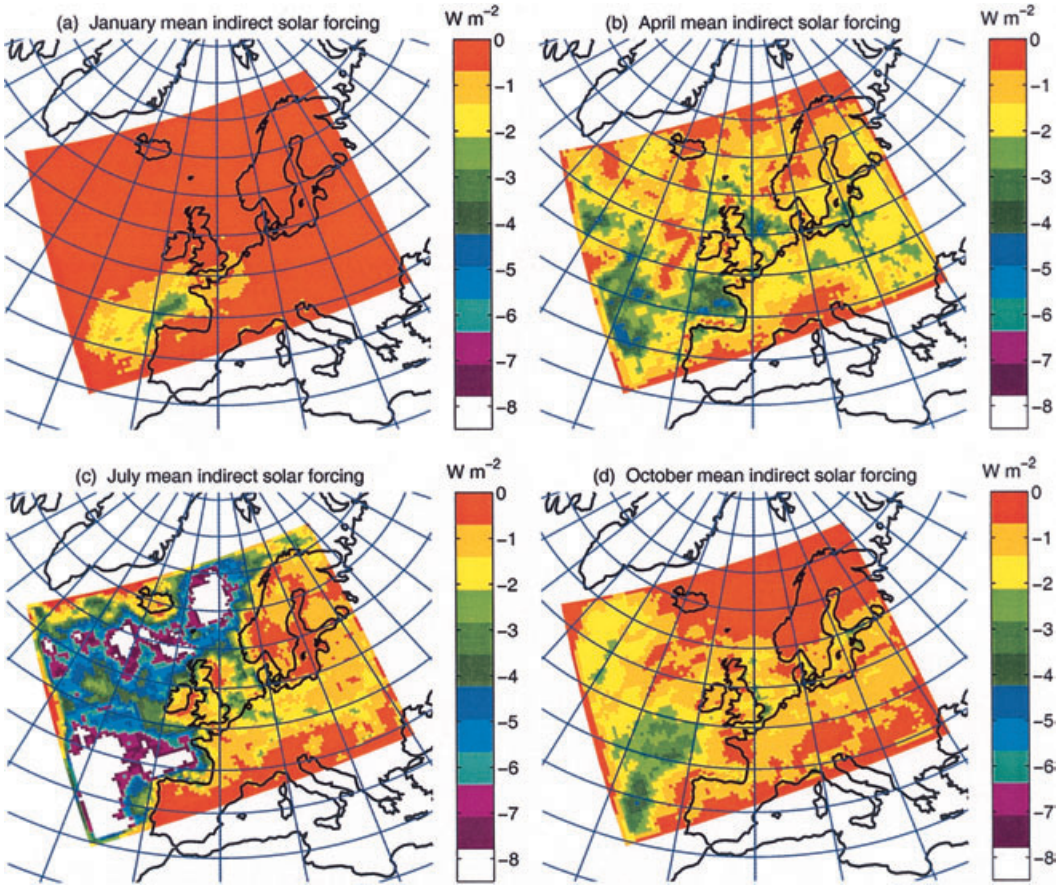

Fig. 8. Spatial distribution of the simulated monthly mean indirect climate forcing (W m^{-2}) due to anthropogenic sulfate aerosols for (a) January, (b) April, (c) July and (d) October.

conducted, some grid-boxes may be cloud-free and values of *LWC* and r_e are missing. Such grid boxes are excluded in the calculations.

If individual grid-points are considered, monthly averages of r_e differ by up to 20–30% between the two resolutions. Averaged over the model domain the difference is less than 7%. There is a tendency to underestimate r_e when 4.0° resolution is used instead of 0.4° resolution, but the bias is not systematic. The change in reflectivity of a cloud is not linearly related to changes in r_e, cf. Fig. 2 in Wyser et al. (1999). Estimated from this figure, a 13% change in r_e from 7.5 to 8.5 μm, with a total cloud condensate amount equal to 30 g m^{-2}, results in only a 5% relative change in cloud reflectivity. In order to obtain a more accurate quantification of the difference in net radiative flux due to the differences in r_e between the two resolutions, complete simulations with a low-resolution version of the RCA2 should be conducted in the future.

4. Sensitivity simulations

Several uncertainties are involved in the modeling of the indirect and direct climate effects, particularly in the former. As demonstrated in Section 3.1.1, the sulfur cycle model element in the RCA2 tends to yield sulfate concentrations that are too low, at least close to the surface. This underestimate is likely to result in too low CDNC from the parameterization in eq. (9) and consequently too large r_e from the parameterization

in eq. (8). On the other hand, the comparison with measurements in Section 3.1.2 showed no sign of an underestimate of CDNC or overestimate of r_e by the model, a result that in turn may be caused by background concentrations of CDNC that are too high. Ekman (2000) concluded that errors in the simulated cloud cover and precipitation might be partly responsible for the scatter in the relation between modeled and observed sulfate concentrations. The simulated cloud liquid water content and cloud cover are also important factors when determining the indirect radiative forcing (cf. Section 3.3). Four sensitivity simulations for the month of July are undertaken with the RCA2 in order to determine the sensitivity of the modeled r_e and indirect radiative forcing results in Section 3 to the uncertainties discussed above.

4.1. *Sensitivity to sulfate concentrations*

The sensitivity of the model to the sulfate concentration is examined by prescribing a doubling of the sulfate concentration in the calculations of r_e [eq. (8)]. This type of change reduces a large part of the bias shown in Fig. 2. The higher sulfate concentration results in an 8% smaller r_e averaged over the model domain (Table 6). Thus, the uncertainty in the sulfate burden does not seem to be the main reason for the discrepancy between satellite observed and modeled r_e seen in Table 3. The overall pattern of indirect radiative forcing due to man-made sulfate remains the same as for the reference case (not shown), whereas the average indirect forcing over the model domain increases by almost 50%, and the maximum radiative forcing is enhanced by 4 W m^{-2} (Table 6). The magnitude of the forcing increase is largest (2–8 W m^{-2}) over the ocean, where the initial background concentration is lowest. Over land, the increase in indirect radiative forcing between the reference and sensitivity simulation varies between 0 and 2 W m^{-2}. A simulation is also performed where the sulfate concentration is halved in the calculations of CDNC. In this case, the average radiative forcing over the model domain decreases by approximately 50%.

Table 6. *Calculated average effective droplet radius and average and maximum change in top-of-the-atmosphere short-wave radiation budget in July for reference and sensitivity simulations*

Simulation	Average r_e^m (μm)	Average indirect forcing (W m^{-2})	Maximum indirect forcing (W m^{-2})
Reference	6.0	−2.6	−14.4
2 × sulfate	5.5	−4.5	−18.2
Low background CDNC	6.4	−5.8	−21.5
High background CDNC	5.8	−1.0	−10.6
Boundary sulfur from ECHAM	5.6	−4.3	−18.0

For explanations of the sensitivity simulations, see text.

4.2. *Sensitivity to background CDNC and cloud liquid water concentration*

The sulfur model only predicts anthropogenic sulfate aerosol mass, whereas the parameterization of CDNC due to Glantz and Noone (2000) requires that the total amount of aerosol mass be known. In the model, background CDNC over ocean and land (equal to 50 and 200 cm^{-3}, respectively) are assumed to which the contribution of man-made sulfate is added. The background concentrations are estimated on the basis of measurements (reported in Section 2.2) that show a large variability. We examine the model's sensitivity to the magnitude of the aerosol background concentration by increasing as well as decreasing $m_{bg,land}$ and $m_{bg,ocean}$ by 50%. This interval encompasses a large part of the variability in the data reported in Covert et al. (1996). The effective droplet radius is inversely proportional to the power one-third of the CDNC and directly proportional to the power one-third of the cloud liquid water content. A 50% change in the CDNC concentration corresponds to a 50% change in the LWC and thus the sensitivity of the model to changes in the LWC is examined at the same time as the background CDNC is varied.

As in Section 4.1, the overall pattern of the indirect radiative forcing due to anthropogenic sulfate is almost unchanged in the sensitivity simulations (not shown). The radiative forcing over the ocean increases by 2–12 W m^{-2} for the lower background concentration (or higher liquid water content) and decreases by 2–7 W m^{-2} for the higher m_{bg} (or lower LWC). Over land the increase is between 0 and 4 W m^{-2} for the low background

CDNC and the decrease is between 0 and 2 W m^{-2} when the background CDNC is enhanced by 50%. The average change in radiative forcing over the whole model domain is approximately doubled for the lower background value of CDNC, whereas it is halved when we use 50% higher background concentrations as compared to the reference case (Table 6). The change in maximum indirect radiative forcing for July is also substantial in the two sensitivity simulations (Table 6).

4.3. Sensitivity to boundary conditions

It has been indicated that sulfur sources outside Europe may be responsible for a substantial part of the total sulfate column burden over the RCA2 model domain (Rasch et al., 2000). In order to account for long-range transport, lateral boundary conditions from a global climate model could be used instead of the zero-boundary condition currently employed in the RCA2. The sensitivity of the modeled sulfur cycle to the boundary conditions of sulfur is tested by utilizing SO_2(a) and SO_4(a) concentrations from the global climate model ECHAM (Feichter and Lohmann, 1999). Data from ECHAM are obtained with a 4-hour time resolution for July 1993.

In the ECHAM simulation of July 1993, the sulfate concentrations are clearly overestimated in the boundary layer compared to the EMEP observations (cf. Feichter and Lohmann, 1999); one reason may be that the simulations are performed using emissions representative of the year 1985. In the free troposphere the concentrations are almost a magnitude higher than in the RCA2 simulation (cf. Section 3.1.1). This difference can only partly be explained by the reduction in emissions between 1985 (as used by ECHAM) and 1996 (as used by RCA2). Applying boundary concentrations from ECHAM on the RCA2 results in a substantial increase of the average sulfate burden, from 2.4 to 9.8 mgSO_4 m^{-2}. It is mainly the concentration in the free troposphere that increases, the tendency of the RCA2 to underestimate sulfate in the boundary layer is not reduced. As mentioned earlier, no observations are available to examine the model's performance outside the boundary layer and since global climate models tend to overestimate the sulfate concentration in the free troposphere (e.g. Barth et al., 2000; Chin et al., 2000), it is difficult to say if the application of lateral boundary conditions from ECHAM actually improves the simulation of sulfate.

The higher sulfate burden yields almost a doubling of the average indirect forcing over the model domain (Table 6). However, the overall forcing pattern still resembles that of the reference simulation.

5. Conclusions

A year-long simulation of the radiative forcing due to man-made sulfate has been conducted with a high-resolution regional climate model (RCA2) including an explicit parameterization of the atmospheric sulfur cycle. Simulated values of cloud liquid water content, relative humidity and fractional cloud cover are utilized in the calculations of the atmospheric sulfur cycle and sulfate aerosol forcing at each time step. No convective transport of sulfur compounds is included in the model, and lateral boundary values of sulfur are set to zero. The main purposes of the study have been to examine the patterns of anthropogenic sulfate climate forcing over Europe, to evaluate modeled key parameters versus observations and to examine the sensitivity of the simulated magnitude and pattern of the indirect climate forcing to key parameters in the parameterizations of the aerosol climate effects.

The overall features of the direct climate forcing in many ways resemble the forcing patterns obtained by previous global and regional climate model studies. However, in contrast to the global models, the regional model is capable of resolving smaller scale phenomena, for example a reduced forcing over the European Alps. Haywood et al. (1997) and Haywood and Boucher (2000) pointed out that sub-grid scale correlations between relative humidity and sulfate not resolved by global climate models may result in an underestimate of the direct climate effect. In the present study, a comparison between the calculated aerosol optical depth at 0.4 and 4° spatial resolution indicates that models with coarse resolution may misrepresent the direct forcing substantially in individual grid-points if sub-grid co-variability is excluded. However, averaged over the model domain, the bias in monthly mean $\tau_{sulfate}$ for the climatic conditions simulated by the RCA2 is only a

few percent, $\tau_{sulfate}$ being smaller at the lower resolution.

One pronounced difference between our regional model results and a previous global climate model simulation by Kiehl et al. (2000), which also considers yearly averages, is that the finer grid spacing in the RCA2 (0.4°) results in a much higher spatial variability of the annual average indirect forcing. Similar variability was reported in the short-term regional model calculations by Langmann et al. (1998). The present calculations show that small-scale forcing maxima exist even on longer time periods than a week. An important question is whether the small-scale indirect forcing variations simulated by the RCA2 are important for the regional temperature and precipitation patterns. In order to obtain an indication of this matter, the effective droplet radius (r_e) is calculated at 0.4 and 4° horizontal resolutions. If individual grid-points are considered, the difference in r_e is substantial between the two resolutions. However, averaged over the model domain, monthly mean values of r_e differ by less than 7%. The change in cloud reflectivity is not linearly related to changes in r_e, but calculations indicate that the smaller r_e obtained with low resolution compared to high resolution would not result in a substantially different net radiative forcing.

An evaluation versus measurements indicates that the model underestimates the sulfate concentration, at least close to the surface. Calculated r_e and CDNC are in good agreement with a limited number of aircraft and surface measurements over the British Isles. A number of similarities can be seen in the gross regional patterns of modeled and satellite-observed r_e. The values of r_e are considerably larger over the ocean than over land; smaller values of r_e are generally found over the North Sea than over the remote Atlantic. The largest r_e are found over the remote Atlantic region and the smallest r_e over Eastern Europe. Satellite-derived values of r_e are considerably larger than modeled. One reason is most likely that the model data are systematically collected at a lower altitude compared to the satellite data due to the limited number of vertical model levels. Furthermore, satellite observations of r_e are not obtained for pixels with partial or inhomogeneous cloud cover.

The magnitude of the average indirect climate forcing over the model domain is highly sensitive to the prescribed background concentrations of CDNC, simulated sulfate aerosol mass and liquid water concentrations. However, the overall pattern of radiative forcing is similar in all sensitivity simulations. In order to reduce the uncertainty of the indirect climate forcing, further evaluation of the model parameterizations versus observational data, especially in the free troposphere, have to be conducted. More long-term, high-quality data on the concentrations of sulfate, CDNC and cloud liquid water are needed for such evaluation.

6. Acknowledgments

I would like to thank my supervisor Henning Rodhe for valuable discussions and comments on the manuscript. I am also most grateful to Ulf Hansson for technical support, Kazuaki Kawamoto for providing the satellite data, Paul Field and the UK Meteorological Office and Meteorological Research Flight for the aircraft data (the Great Dunn Fell experiment was financed by the Natural Environment Research Council), Colin Jones for providing the cloud comparison data and Erik Kjellström for providing sulfur boundary data from ECHAM. Financial support has been obtained from the Swedish Regional Climate Modeling Programme (SWECLIM) funded by MISTRA and SMHI. Model simulations were conducted on the Cray T3E at the Swedish National Supercomputing Center.

7. Appendix A

Following Savijärvi (1990), the net short-wave radiative flux divergence $\partial F_{s,net}/\partial p$ over a certain layer is proportional to the temperature tendency $\partial T/\partial t_s$ according to

$$\frac{\partial T}{\partial t_s} = -\frac{g}{c_p}\frac{\partial F_{s,net}}{\partial p}, \tag{A1}$$

where g is the acceleration of gravity and c_p the specific heat capacity at constant pressure. Furthermore,

$$\frac{\partial T}{\partial t_s} = \frac{\partial T}{\partial t_{sa}}(1 - C_M) + \frac{\partial T}{\partial t_{sc}} C_M, \tag{A2}$$

where the first term on the right-hand side of the

equation represents absorption in clean air and the second term absorption in cloudy air. As an approximation, the cloudy fraction of the grid-box C_M is set to be equal to the maximum fraction cloud cover of all levels in a vertical column.

The heating rate of the clear air is equal to

$$\frac{\partial T}{\partial t_{sa}} = S\frac{q}{c_p}\frac{p}{p_{00}}[Y(u_s) + 1.67\alpha\cos\theta \times Y(u_*)] + 1.7e10\cos\theta^{0.3}, \quad \text{(A3)}$$

$$Y(u_s) = \begin{cases} 0.03u_s^{-0.81}, & u_s \geqslant 0.05 \text{ cm} \\ 0.05u_s^{-0.63}, & u_s < 0.05 \text{ cm} \end{cases}, \quad \text{(A4)}$$

where u_s is the pressure-scaled slant water vapor path [cf. eq. (2)], S is the TOA solar flux, q is the relative humidity, p is the pressure, p_{00} is a reference pressure (1000 hPa), α is the short-wave albedo of the ground, θ is the solar zenith angle and b_1–b_4 are constants. The path length for isotropically reflected beams is

$$u_* = \frac{1}{\cos\theta}u(0, p_s) + 1.67u(p, p_s), \quad \text{(A5)}$$

where p_s is the surface pressure. The cloud absorption is given by

$$\frac{\partial T}{\partial t_{sc}} = \hat{T}(p_z, p)\frac{\partial T}{\partial t_{sa}} + \frac{g}{c_p}F_{sz}\frac{\partial}{\partial p}\hat{A}(p_z, p), \quad \text{(A6)}$$

where index z denotes the uppermost cloud layer, F_{sz} is the solar flux density, $\hat{T}$ is the transmittance factor for the cloudy atmosphere above and $\hat{A}$ is the absorption factor. The following expressions have been fitted to cloud absorption and transmission computations obtained from more detailed schemes

$$\hat{A} = 0.013(1.4 + \cos\theta) \times \ln(1 + 0.10M_t), \quad \text{(A7)}$$

$$\hat{T} = \frac{\hat{T}_l}{(\hat{T}_l + M_t)}, \quad \hat{T}_l = 40(0.5 + \cos\theta). \quad \text{(A8)}$$

M_t is the vertically integrated cloud water from the top of the uppermost cloud layer to a level below.

REFERENCES

Albrecht, B. A. 1989. Aerosols, cloud microphysics, and fractional cloudiness. *Science* **245**, 1227–1230.

Barth, M. C., Rasch, P. J., Kiehl, J. T., Benkovitz, C. M. and Schwartz, S. E. 2000. Sulfur chemistry in the National Center for Atmospheric Research Community Climate Model: description, evaluation, features and sensitivity to aqueous chemistry. *J. Geophys. Res.* **105**, 1387–1415.

Berge E. 1990. A regional numerical sulfur dispersion model using a meteorological model with explicit treatment of clouds. *Tellus* **42B**, 389–407.

Berge, E. 1993. Coupling of wet scavenging of sulphur to clouds in a numerical weather prediction model. *Tellus* **45B**, 1–22.

Benkovitz, C. M., Scholtz, M. T., Pacyna, J., Tarrason, L., Dignon, J., Voldner, E. C., Spiro, P. A., Logan, J. A. and Graedel, T. E. 1996. Global gridded inventories of anthropogenic emissions of sulfur and nitrogen. *J. Geophys. Res.* **101**, 29,239–29,253.

Bott, A. 1989a. A positive definite advection scheme obtained by nonlinear renormalization of the advected fluxes. *Mon. Wea. Rev.* **117**, 1006–1015.

Bott, A. 1989b. Reply. *Mon. Wea. Rev.* **117**, 2633–2636.

Boucher, O. and Lohmann, U. 1995. The sulfate–CCN–cloud albedo effect: a sensitivity study with two general-circulation models. *Tellus* **47B**, 281–300.

Charlson, R. J., Langner, J., Rodhe, H., Leovy, C. B. and Warren, S. G. 1991. Perturbation of the northern hemisphere radiative balance by backscattering from anthropogenic sulfate aerosols. *Tellus* **4B3**, 152–163.

Charlson, R. J., Anderson, T. L. and Rodhe, H. 1999. Direct climate forcing by anthropogenic aerosols: Quantifying the link between atmospheric sulfate and radiation. *Contr. Atmos. Phys.* **72**, 79–94.

Chin, M., Savoie, D. L., Huebert, B. J., Bandy, A. R., Thornton, D. C., Bates, T. S., Quinn, P. K., Saltzman, E. S. and De Bruyn, W. J. 2000. Atmospheric sulfur cycle simulated in the global model GOCART: Comparison with field observations and regional budgets. *J. Geophys. Res.* **105**, 24,689–24,712.

Choularton, T. W., Bower, K. N., Beswick, K. M., Parkin, M. and Kaye, A. 1998. A study of the effects of cloud processing of aerosol on the microphysics of cloud. *Q. J. R. Meteorol. Soc.* **124**, 1377–1389.

Chuang, C. C., Penner, J. E., Taylor, K. E., Grossman, A. S. and Walton, J. J. 1997. An assessment of the radiative effects of anthropogenic sulfate. *J. Geophys. Res.* **102**, 3761–3778.

Covert, D. S., Wiedensohler, A., Aalto, P., Heintzenberg, J., McMurry, P. H. and Leck, C. 1996. Aerosol number size distributions from 3 to 500 nm diameter in the Arctic marine boundary layer during summer and autumn. *Tellus* **48B**, 197–212.

Curry, J. A. 1986. Interactions among turbulence, radiation and microphysics in Arctic stratus clouds. *J. Atmos. Sci.* **43**, 90–106.

Cuxart, J., Bougeault, P. and Redelsperger, J.-L. 2000. A turbulence scheme allowing for mesoscale and large-eddy simulations. *Q. J. R. Meteorol. Soc.* **126**, 1–30.

Eerola K., Salmond D., Gustafsson N., Garcia-Moya J.-A., Lönnberg P. and Järvenoja S. 1997. A parallel version of the HIRLAM forecast model: Strategy and results. In: *Making its mark* (eds. Hoffman, G.-R. and Kreitz N.), Proceedings of the seventh ECMWF Workshop of the use of Parallel Processors in Meteorology. Reading, UK, November, 1996, 134–143.

Ekman, A. 2000., Implementation of an atmospheric sulfur scheme in the HIRLAM regional weather forecast model. *Report CM-96*, International Meteorological Institute in Stockholm, Department of Meteorology, Stockholm University, S-10691 Stockholm, Sweden.

Feichter, J. and Lohmann, U. 1999. Can a relaxation technique be used to validate clouds and sulphur species in a GCM? *Q. J. R. Meteorol. Soc.* **125**, 1277–1294.

Feichter, J., Lohmann, U. and Schult, I. 1997. The atmospheric sulfur cycle in ECHAM-4 and its impact on the shortwave radiation. *Clim. Dyn.* **13**, 235–246.

Glantz, P. and Noone, K. J. 2000. A physically based algorithm for estimating the relationship between aerosol mass and cloud droplet number. *Tellus* **52B**, 1216–1231.

Hass, H., Berge, E., Ackermann, I., Jakobs, H. J., Memmesheimer, M. and J.-P.Tuovinen, A diagnostic comparison of EMEP and EURAD. Model results for a wet deposition episode in July 1990. *EMEP/MSC-W Report 4/96*, The Norwegian Meteorological Institute, Oslo, Norway, 1996.

Haywood, J. M. and Boucher, O. 2000. Estimates of the direct and indirect radiative forcing due to tropospheric aerosols: a review. *Rev. Geophys.* **38**, 513–543.

Haywood, J. M., Ramaswamy, V. and Donner, L. J. 1997. A limited-area-model case study of the effects of subgrid scale variations in relative humidity and cloud upon the direct radiative forcing of sulfate aerosol. *Geophys. Res. Lett.* **24**, 143–146.

Herman, G. F. and Curry, J. A. 1984. Observational and theoretical studies of solar radiation in Arctic stratus clouds. *J. Appl. Meteorol.* **23**, 5–24.

Hegg, D. A. 1994. Cloud condensation nucleus-sulfate mass relationship and cloud albedo. *J. Geophys. Res.* **99**, 25,903–25,907.

Hjellbrekke, A. G. and Hanssen, J. E. 1998. Data report 1996, Part 2. Monthly and seasonal summaries. *NILU/CCC-report 2/98*, pp 229. The Norwegian Institute for Air Research, Lillestrøm, Norway.

Intergovernmental Panel on Climate Change (IPCC), 1996. *Climate change, 1995: the science of climate change* (ed. J. T. Houghton et al.), Cambridge University Press, New York, 572 pp.

Jennings, S. G., Geever, M., McGovern, F. M., Francis, J., Spain, T. G. and Donaghy, T. 1997. Microphysical and physio-chemical characterization of atmospheric and continental aerosol at Mace Head. *Atmos. Environ.* **31**, 2795–2808.

Jones, A. and Slingo, A. 1996. Predicting cloud-droplet effective radius and indirect sulphate aerosol forcing using a general circulation model. *Q. J. R. Meteorol. Soc.* **122**, 1573–1595.

Jones, A., Roberts, D. L. and Slingo, A. 1994. A climate model study of indirect radiative forcing by anthropogenic sulphate aerosols. *Nature* **370**, 450–453.

Kain, J. S. and Fritsch, J. M. 1990. A one-dimensional entraining/detraining plume model and its application in convective parameterization. *J. Atmos. Sci.* **47**, 2784–2802.

Källén, E. (ed.), 1996. *HIRLAM documentation manual – System 2.5*. Available from the Swedish Meteorological and Hydrological Institute, SE-60176 Norrköping, Sweden, 240 pp.

Kawamoto, K., Nakajima, T. and Nakajima, T. 2001. A global determination of cloud microphysics with AVHRR remote sensing. *J. Clim.* **14**, 2054–2068.

Kiehl, J. T., Hack, J. J., Bonan, G. B., Boville, B. A., Williamson, D. L. and Rasch, P. J. 1998. The National Center for Atmospheric Research Community Climate Model: CCM3. *J. Clim.* **11** 1131–1150.

Kiehl J. T., Schneider, T. L., Rasch, P. J. and Barth, M. C. 2000. Radiative forcing due to sulfate aerosols from simulations with the National Center for Atmospheric Research. Community Climate Model, Version 3. *J. Geophys. Res.* **105**, 1441–1457.

Koch, D., Jacob, D., Tegen, I., Rind, D. and Chin, M. 1999. Tropospheric sulfur simulation and sulfate direct radiative forcing in the Goddard Institute for Space Studies general circulation model. *J. Geophys. Res.* **104**, 23,799–23,822.

Kotchenruther, R. A., Hobbs P. V. and Hegg, D. A. 1999. Humidification factors for atmospheric aerosols off the mid-Atlantic coast of the United States. *J. Geophys. Res.* **104**, 2239–2251.

Langmann, B., Herzog, M. and Graf, H.-F. 1998. Radiative forcing of climate by sulfate aerosols as determined by a regional circulation chemistry transport model. *Atmos. Environ.* **32**, 2757–2768.

Lohmann, U. and Feichter, J. 1997. Impact of sulfate aerosols on albedo and lifetime of clouds: a sensitivity study with the ECHAM4 GCM. *J. Geophys. Res.* **102**, 13,685–13,700.

Lohmann, U., Feichter, J., Chuang, C. C. and Penner, J. E. 1999a. Prediction of the number of cloud droplets in the ECHAM GCM. *J. Geophys. Res.* **104**, 9169–9198.

Lohmann, U., Feichter, J., Chuang, C. C. and Penner, J. E. 1999b. Correction to 'Prediction of the number of cloud droplets in the ECHAM GCM. *J. Geophys. Res.* **104**, 24,557–24,563.

Mahowald, N. M, Rasch, P. J., Eaton, B. E., Whittlestone, S and Prinn, R. G. 1997. Transport of ^{222}radon to the remote troposphere using the Model of Atmospheric Transport and Chemistry and assimilated winds from ECMWF and the National Center

for Environmental Prediction/NCAR. *J. Geophys. Res.* **102**, 28,139–28,151.

Martin, G. M., Johnson, D. W. and Spice, A. 1994. The measurement and parameterization of effective radius of droplets in warm stratocumulus clouds. *J. Atmos. Sci.* **51**, 1823–1842.

Mylona, S. 1999. EMEP emission data. Status Report 1999. *EMEP/MSC-W Note 1–99*, Norwegian Meteorological Institute, Oslo, Norway.

New, M., Hulme, M. and P. Jones. Representing twentieth-century space-time climate variability, Part I. Development of a 1961–90 mean monthly terrestrial climatology. *J. Clim.* **12**, 829–856.

Patterson, E. M., Kiang, C. S., Delany, A. C., Wartburg, A. F., Leslie, A. C. D. and Huebert, B. J. 1980. Global measurements of aerosols in remote continental and marine regions: Concentrations, size distributions, and optical properties. *J. Geophys. Res.* **85**, 7361–7376.

Penner, J. E., Chuang, C. C. and Grant, K. 1998. Climate forcing by carbonaceous and sulfate aerosols. *Clim. Dyn.* **14**, 839–851.

Pirjola, L., Laaksonen, A., Aalto, P. and Kulmala, M. 1998. Sulfate aerosol formation in the Arctic boundary layer. *J. Geophys. Res.* **103**, 8309–8321.

Rasch, P. J. and Kristjánsson, J. E. 1998. A comparison of the CCM3 model climate using diagnosed and predicted condensate parameterizations. *J. Clim.* **11**, 1587–1614.

Rasch, P. J., Barth, M. C., Kiehl, J. T., Schwartz, S. E. and Benkovitz, C. M. 2000. A description of the global sulfur cycle and its controlling processes in the National Center for Atmospheric Research Community Climate Model, Version 3. *J. Geophys. Res.* **105**, 1367–1385.

Roeckner, E., Bengtsson, L. and Feichter, J. 1999. Transient climate change simulations with a coupled atmosphere–ocean GCM including the tropospheric sulfur cycle. *J. Clim.* **12**, 3004–3032.

Roelofs, G-J., Lelieveld, J. and Ganzeveld, L. 1998. Simulation of global sulfate distribution and the influence on cloud drop radii with a coupled photochemical sulfur cycle model. *Tellus* **50B**, 224–242.

Rosenfeld, D. 2000. Suppression of rain and snow by urban and industrial air pollution. *Science* **287**, 1793–1796.

Rummukainen, M., Räisänen, J., Bringfelt, B., Ullerstig, A., Omstedt, A., Willén, U., Hansson, U. and Jones, C. 2001. A regional climate model for northern Europe – model description and results from the downscaling of two GCM control simulations. *Clim. Dyn.* **5/6**, 339–359.

Räisänen, P., Rummukainen, M. and Räisänen, J. 2000. Modification of the HIRLAM radiation scheme for use in the Rossby Centre regional atmospheric climate model. *Report No. 49*. Department of Meteorology, University of Helsinki, Finland.

Savijärvi, H. 1990. Fast radiation parameterization schemes for mesoscale and short-range forecast models. *J. Appl. Meteor.* **29**, 437–447.

Simmons, A. J. and Burridge, D. M. 1981. An energy and angular momentum conserving vertical finite-difference scheme and hybrid vertical coordinates. *Mon. Wea. Rev.* **109**, 758–766.

Twomey, S. 1974. Pollution and the planetary albedo. *Atmos. Environ.* **8**, 1251–1256.

World Climatic Program, 1986. A preliminary cloudless standard atmosphere for radiation computation (ed. H. E. Gerber). *Ser. Rep.* **112**, Int. Counc. Sci. Unions and World Meteorological Organization, Geneva, Switzerland.

Wyser, K., Rontu, L. and Savijärvi, H. 1999. Introducing the effective radius into a fast radiation scheme of a mesoscale model. *Contr. Atmos. Phys.* **72**, 205–218.